Available online at www.sciencedirect.com
ScienceDirect
Energy Reports 8 (2022) 1464–1478
www.elsevier.com/locate/egyr

TMREES22-Fr, EURACA, 09 to 11 May 2022, Metz-Grand Est, France

Coherence of digital processing of current and voltage signals at decimation for power systems with a large share of renewable power stations

A.L. Kulikov[a], P.V. Ilyushin[a,*], K.V. Suslov[b], D.N. Karamov[a]

[a] *Energy Research Institute of the Russian Academy of Sciences (ERI RAS), Nagornaya st. 31/2, Moscow, 117186, Russia*
[b] *Irkutsk National Research Technical University (INRTU), Lermontov st. 83, Irkutsk, 664074, Russia*

Received 16 August 2022; accepted 17 August 2022
Available online xxxx

Abstract

The high energy and environmental performance of renewable power stations (RPS) contributes to their widespread introduction in many countries. A trend towards decentralization of generating capacities and an increase in the share of RPS in their structure brings about the multifactorial features that affect the reliability of power systems. These factors can result in a failure and unnecessary or false operation of intelligent digital devices and systems that perform the protection and automatic control functions. Digital substations using the IEC 61850 protocol to exchange instantaneous values of analog signals employ merging units (MUs) for digital processing of current and voltage. MUs use down-sampling, i.e., decimation, to reduce the number of calculations and meet other purposes. The paper presents findings of an analysis of the digital processing effects associated with the disturbance of coherence of current and voltage signals during decimation. Failure to comply with the coherence requirements during decimation leads to significant errors in the estimates of signal parameters. The extent to which the sinusoidality of signals is distorted due to incoherence can be determined using a normalized cross-correlation coefficient. Simulation results have shown that incoherent sampling enhances the distorting effect for the signals containing high-frequency harmonics and interharmonics. Coherence of digital signal processing after decimation can be ensured by preliminary digital filtering. Superposition of noise components does not affect much the estimations of signal amplitudes during decimation, which are within the allowable error. Coherence of digital processing of current and voltage signals during decimation contributes to the reliable operation of power systems with a large share of RPS, first of all solar photovoltaic and wind power stations.

Peer-review under responsibility of the scientific committee of the TMREES22-Fr, EURACA, 2022.

Keywords: Renewable power stations; Digital signal processing; Coherence; Decimation; Distorting effect; Normalized cross-correlation coefficient; Phase relation

1. Introduction

In recent years, the global power industry has been involved in organizational and technical activities to transform power systems fundamentally. Many countries are developing renewable power stations (RPS) due to their high

* Corresponding author.
E-mail address: ilyushinpv@list.ru (P.V. Ilyushin).

https://doi.org/10.1016/j.egyr.2022.08.215

Peer-review under responsibility of the scientific committee of the TMREES22-Fr, EURACA, 2022.

energy and environmental efficiency, which helps to reduce dependence on gas and oil imports. A steady trend towards a decrease in specific capital investments in the construction of RPS contributes to their widespread introduction in power systems (Razavi et al. 2019 [1]; Singh and Sharma, 2017 [2]; Mehigana et al. 2018 [3]; Zeng et al. 2016 [4]).

A report by Bloomberg NEF and the United Nations Environment Program notes that over the past ten years, more generating capacities have been added to wind and solar power plants than any other type of energy source. Some countries plan to completely transition to electricity generation only from equipment based on renewable energy sources, for example, Sweden by 2040 and Canada by 2050.

In Russia, the share of wind (WPSs) and solar photoelectric (SPVSs) plants by the end of 2024 is expected to be about 2% of the total installed capacity of all generating equipment and about 0.8% of the total electricity generation (Ilyushin et al. 2021 [5]). Given the restrictions on power flows between the interconnected power systems (IPSs) and regional power systems, it is necessary to analyze the size of WPSs and SPVSs capacities in each of them separately at the level of regional energy systems. In the IPS of the South, with a total installed capacity of generating equipment at thermal power plants (TPPs), hydroelectric power plants (HPPs), nuclear power plants (NPPs), and pumped storage power plants (PSPPs) of 24.8 GW, the installed capacity of WPSs and SPVSs will be 3.6 GW, i.e., 14.5%, by the end of 2024, while the available control range at TPPs will significantly decrease. In 2022, in the Republic of Kalmykia, with the installed capacity of the thermal power plant equal to 18 MW, after commissioning the second start-up complex at the Arshan SPVS (37.6 MW), the installed capacity will be 450.7 MW with maximum power consumption of 124 MW (Degtyarev, 2017 [6]).

A crucial way to transform the power industry is the gradual smartization of power systems. The development and adoption of intelligent digital devices and systems (IDDSs) should increase the reliability, safety, and efficiency of control of power systems. However, the IDDSs bring about new problems due to the complication of power systems and a decrease in the level of self-adaptation and self-resilience to a whole host of destabilizing factors (Voropai et al. 2018 [7]; Papkov B. et al. 2015 [8]; Voropai et al. 2019 [9]).

It is known that to comply with the requirements, power systems are equipped with IDDSs that perform various functions, including protection and automatic control. The main purpose of protection and automatic systems is to quickly identify and reliably and selectively disable damaged components to prevent the development of accidents (Ilyushin and Pazderin, 2018 [10]). Processing discrete, as well as digital, current and voltage signals of power frequency in IDDSs requires a reduction or an increase in the sampling rate. Change in the sampling rate provides an opportunity to simplify the software and hardware implementations of narrow-band digital filters (Rabiner and Gold, 1975 [11]; Oppenheim and Schafer, 2009 [12]; Ribeiro et al. 2014 [13]).

Sampling rate reduction by sample decimation is used by manufacturers of IDDSs designed for digital substations that exchange instantaneous values (SV - streams) to reduce the number of calculations.

With the IDDS support of the data exchange protocol according to the IEC 61850 SV standard, the sampling rate is normally reduced by a factor of 4, i.e., 20 instead of 80 samples are used per power frequency period. The paper presents the results of analysis for the effects of digital signal processing associated with the incoherence of power frequency current and voltage signals, which occurs during decimation (Borkowski, 2007 [14]; Khan Shabbir and Liang, 2020 [15]; Graham and Lediju Bell, 2020 [16]).

The paper aims to present avenues to ensure the coherence of digital processing of current and voltage signals in IDDSs during decimation. This is necessary to prevent unnecessary and false operation of IDDSs, which perform the functions of protection and automatic control, to provide the reliable operation of power systems with a large share of RPSs.

2. Specific features of transient processes in energy systems with renewable power stations

The decentralization of generating capacities and the large-scale adoption of generation systems based on renewable energy sources leads to the specific features that have a significant impact on the capability of ensuring reliable operation of power systems:

- permanent fluctuations of the power flow parameters in a wide dynamic range in the case of a large share of generation systems based on renewable energy sources characterized by a stochastic nature of electricity generation,
- significant deviations of power quality indices from standard values, especially in low-load modes of equipment with power electronics elements (RPS inverters/converters),

- the nature and parameters of transient processes are determined by the load characteristics, given the low mutual electrical resistance, and the fact that the total load value in load centers is comparable with the total power of generating plants, including RPSs (Ilyushin, 2017 [17]; Gurevich and Libova, 2008 [18]),

- high speeds of electromechanical transient processes caused by a decrease in the equivalent inertia constant of the rotating masses of gensets in power systems (load centers),

- significant deviations of operating parameters during emergency disturbances accompanied by the shutdown of generating plants, including RPS, and consumer loads sensitive to such deviations (Gurevich et al. 1990 [19]).

In the current stage, the above specific features manifest themselves clearly in the islanded and off-grid operation of individual energy system sections (Eroshenko and Ilyushin, 2018 [20]).

At the same time, one of the most important problems for SPVSs today is the problem of correctly determining the output parameters of the SPVS photovoltaic part, the influence of specific operating conditions on them, and the compliance of the declared values of these parameters with the actual values at the place of operation (Izmailov et al. 2019 [21], Shepovalova, 2019 [22], Izmailov et al. 2018 [23], Strebkov et al. 2019 [24]).

Thus, voltages at nodes and currents in the branches of power systems are not ideally sinusoidal since they contain various harmonic and noise components even in steady-state conditions. Emergency disturbances are always accompanied by electromechanical and electromagnetic transients, with possible oscillations and resonance phenomena characterized by a dramatic change in the amplitude of currents and voltages of power frequency and the phase angle.

The algorithms for estimating the parameters of currents and voltages based on the discrete Fourier transform (DFT), which are currently used in most measuring devices of the IDDSs, assume a sinusoidal signal model that does not change in the data window (Ren and Kezunovic, 2012 [25]). Therefore, in transient processes with frequency fluctuations, when current and voltage signals contain modulation components and jumps in amplitude and phase angle are observed, there will be significant errors in estimating their values.

In Serna and Martin, 2003 [26] the authors have proposed an improved cosine filtering algorithm that provides accurate results in cases where current and voltage signals are subject to amplitude modulation. The algorithm relies on polynomial transformations to approximate changes in amplitude and phase angle, which allow describing the envelope with a greater degree of approximation. The study discussed in Serna, 2007 [27], develops the idea presented in Serna and Martin, 2003 [26], and considers the application of the Taylor polynomial model to improve the accuracy of measurements under power fluctuations. In Kulikov and Lukicheva, 2018 [28], the authors propose using multiparameter dynamic models with subsequent DFT error compensation.

The research of Ribeiro et al. 2014 [13], Ren and Kezunovic, 2012 [25] notes that step changes in amplitude and phase angle can occur inside the data window due to electromagnetic transients during the digital processing of power frequency signals. This can significantly affect the signal parameter estimation due to the "break" of the functional time dependence of the sinusoidal signal, which in the general case corresponds neither to a previous normal nor subsequent emergency condition. Jumps of instantaneous current and voltage values are possible in the case of equipment damage with arc overvoltage, operational switching, or significant changes in weather conditions that affect the operating conditions of generation systems based on renewable energy sources. In this case, estimates of current and voltage parameters may prove invalid and, for example, slow down or postpone the generation of control actions in the IDDSs, which can cause a malfunction of the operation of protection and automatic control.

In light of the considered features of transient processes, reliable operation of power systems with a large share of RPS can only be provided if the IDDS protection and automatic control functions work correctly. It is worthwhile to note that the digital signal processing methods used in IDDS may function incorrectly in the case of electromechanical and electromagnetic transients due to distortions in sinusoidality of power frequency current and voltage (Antonov, 2018 [29]).

Sinusoidality can also be violated in the event of synchronous oscillations related to the upset power balance in some parts of the power system due to connection (tripping) of power lines, large generating plants including RPS, or significant amounts of load. With synchronous oscillations caused by electromechanical transients, the amplitude and phase of the angle between current and voltage are modulated by a low-frequency signal, which corresponds to the instantaneous slips of synchronous machines (Buchholz and Styczynski, 2014 [30]; Shushpanov et al. 2021 [31]).

Fig. 1 shows an example of an oscillogram recorded by WAMS, where one can see low-frequency active power fluctuations in the power system, which last 12 min, with a frequency of 0.9 Hz and an amplitude of 20 to 80 MW.

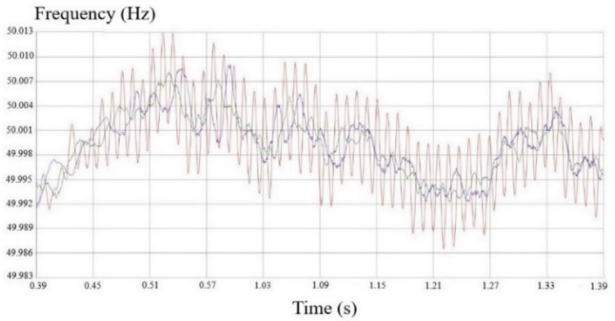

Fig. 1. Oscillogram of synchronous swings in the power system.

There are numerous cases of significant deviations of operating parameters in the islanded or isolated network areas in the event of emergency disturbances: two-phase or three-phase short circuits in the electrical network area; load shedding of more than 30% of the total generating capacity, including RPS; direct start of a group of asynchronous motors with a total power of more than 30% of the total power of generating plants, including RPS.

3. Specific features of digital signal processing in the case of decimation

Devices that perform decimation belong to the so-called descending discrete systems, in which the sampling rate of the signal at the output F_{S1} is lower than the sampling rate at the input F_S (Goldenberg et al. 1985 [32]).

The typical structure of the elementary descending discrete system is shown in Fig. 2 (T_S – sampling interval; $T_S = 1/F_S$). It includes a filtering module that preprocesses the input signal with a sampling rate F_S and a decimation module that reduces the sampling rate by m times—to F_{S1}. Both modules are usually part of a digital signal processing device, i.e., a merging unit.

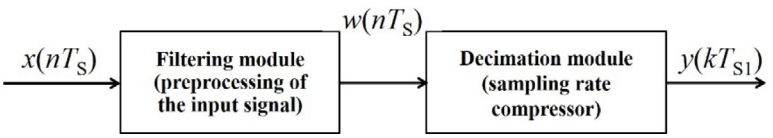

Fig. 2. Typical structure of the elementary descending discrete system (MU).

The filtering module (see Fig. 2) is necessary to prevent or reduce the aliasing that occurs during the decimation of current and voltage signals, the features of which are given further in the paper.

We will consider the connection between the input and output sequences of the decimation module. In this case, the preprocessing procedure in the filtering module is described by the equation (Rabiner and Gold, 1975 [11]; Oppenheim and Schafer, 2009 [12])

$$w(n) = \sum_{l=0}^{n} h(l) \cdot x(n-l) \tag{1}$$

where $w(n)$ is the output signal of the filtering module, n is the current sample index, l is the impulse response index of the filtering module and $h(l)$ is an impulse response of the filtering module.

Note that digital signal processing in a conventional linear filter (Eq. (1)) can be interpreted as the summation of the input sequence $x(n)$ in a window sliding through one sample $h(n)$.

The decimation module samples the signals at time points $t = nm\ T_S$, where $n = 0, 1, 2$. In doing so, each mth sample is taken from the input signal $w(nT_S)$ coming from the filtering module. The signal in the process of decimation is decimated, and sampling is carried out with a large sampling interval equal to $T_{S1} = mT_S$, as shown in Fig. 3 (at the decimation module output).

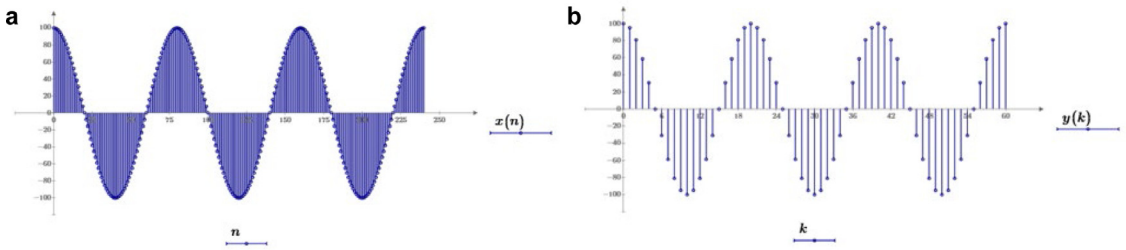

Fig. 3. Oscillograms of sinusoidal signal before decimation (a) and after decimation (b).

Then the general equation describing the operation of the descending discrete system (Fig. 2) takes the form (Rabiner and Gold, 1975 [11]; Oppenheim and Schafer, 2009 [12])

$$y(k) = w(km) = \sum_{l=0}^{km} h(l) \cdot x(n-l) \tag{2}$$

where k is the current sample index at the system output.

Processing by down sampling (Eq. (2)) is a summation in a window $h(n)$ "jumping" over m samples.

Analysis of Eq. (2) shows that the decimation procedure implements digital signal processing that is not invariant to time shift and has m different impulse characteristics (responses to the input sequence in the form of a discrete δ-function).

To identify the specific features of digital processing, we will analyze the spectra of signals during decimation using Z-transforms of sequences $w(n)$ and thinned $y(k)$ (Rabiner and Gold, 1975 [11])

$$W(z) = \sum_{n=0}^{\infty} w(n) z^{-n} \tag{3}$$

$$Y(z_1) = \sum_{k=0}^{\infty} y(k) z_1^{-k} \tag{4}$$

Let us determine the spectral components by substitution (Rabiner and Gold, 1975 [11])

$$z = e^{j2\pi f T_S} \quad \text{and} \quad z_1 = e^{j2\pi f m T_{S1}} = e^{j2\pi f m T_S} \tag{5}$$

where f is the frequency, z and z_1 is the spectral components of signals before decimation and after decimation respectively.

It follows from the last expression that (Rabiner and Gold, 1975 [11]; Oppenheim and Schafer, 2009 [12])

$$z_1 = z^m \quad \text{and} \quad Y(z^m) = \sum_{k=0}^{\infty} y(k) z_1^{-mk} \tag{6}$$

Consider the sum

$$\sum_{p=0}^{m-1} W\left(z \cdot e^{\frac{j2\pi p}{m}}\right) \tag{7}$$

where p is the spectral components summation index.

To establish relation between $W(z)$ and $Y(z_1)$, transform Eq. (3) into the form

$$\sum_{p=0}^{m-1} W\left(z \cdot e^{\frac{j2\pi p}{m}}\right) = \sum_{p=0}^{m-1} \sum_{n=0}^{\infty} w(n) z^{-n} \cdot e^{-\frac{j2\pi pn}{m}} = \sum_{n=0}^{\infty} \left(\sum_{p=1}^{m-1} e^{-\frac{j2\pi pn}{m}} \right) w(n) z^{-n} \tag{8}$$

The sum in brackets is the sum of m terms of the geometric progression with the first term equal to $e^{-\frac{j2\pi pn}{m}}$. Hence,

$$\sum_{p=0}^{m-1} e^{-\frac{j2\pi pn}{m}} = \begin{cases} m \text{ at } n = km, \ k = 0, 1, 2, \ldots \\ 0 \text{ at other } n \end{cases} \tag{9}$$

Substitution Eq. (9) into Eq. (8) and replacement $n = km$ yields the expression

$$\sum_{p=0}^{m-1} W\left(z \cdot e^{\frac{j2\pi p}{m}}\right) = m \sum_{k=0}^{\infty} w(km) z^{-km} = m \sum_{k=0}^{\infty} y(k) z_1^{-k} = mY(z_1) \tag{10}$$

Thus, the relation between the Z-transforms of the original and thinned sequences corresponds to the equality

$$Y(z) = \frac{1}{m} \sum_{p=0}^{m-1} W\left(z \cdot e^{\frac{j2\pi p}{m}}\right) \tag{11}$$

and passing to the spectra by substituting Eq. (5) into Eq. (11), we obtain

$$Y(e^{j2\pi f T_{S_1}}) = \frac{1}{m} \sum_{p=0}^{m-1} W e^{j2\pi T_S\left(f + \frac{p}{mT_S}\right)} \tag{12}$$

Analysis of Eq. (12) allows the conclusion that the spectrum of the output signal of the decimation module is the sum of the input signal spectra shifted relative to each other along the frequency axis by the value $1/mT_S$

$$Y(j2\pi f) = \frac{1}{m} \sum_{p=0}^{m-1} W\left(j2\pi\left(f + \frac{p}{mT_S}\right)\right) \tag{13}$$

Thus, there will be no superposition of spectra during decimation if the signal spectrum at the decimation module output occupies the bandwidth

$$-\frac{\pi}{mT_S} < 2\pi f < \frac{\pi}{mT_S} \tag{14}$$

The spectrum of the output signal from the filtering module (Fig. 2) is the product of the spectra of the input signal $x(nT_S)$ and frequency response of the filter (H_F) implemented in this module

$$W(j2\pi f) = X(j2\pi f) \cdot H_F(j2\pi f) \tag{15}$$

Substituting the results from Eq. (15) into Eq. (13), we obtain an expression relating the spectra of the input and output signals of the decimation module

$$Y(j2\pi f) = \frac{1}{m} \sum_{p=0}^{m-1} X\left(j2\pi\left(f + \frac{p}{mT_S}\right)\right) \cdot H_F\left(j2\pi\left(f + \frac{p}{mT_S}\right)\right). \tag{16}$$

The first term in Eq. (16) (corresponding to $p = 0$) is equivalent to the spectrum of the useful thinned signal. The remaining terms violate the coherence of digital signal processing, and they can be considered as interference spectra that distort the useful signal in the base band (Fig. 4) (Hu and Lee, 2014 [33]).

Analysis of Fig. 4 suggests that a mandatory prerequisite for the coherence and adequacy of digital signal processing is the required suppression by filtering module of the distorting components of the spectrum outside the main signal band, determined by Eq. (14) (Li et al. 2021 [34]).

4. Model experiments with oscillograms currents and voltages

Let us develop a program for experimental research based on the principles of the implementation of the IDDS measuring elements. We set analytically the current and voltage oscillograms in combination with the impact of the following distorting factors:

- additive components of currents and voltages in the form of multiple harmonic components and interharmonics of various intensities and spectral ranges,

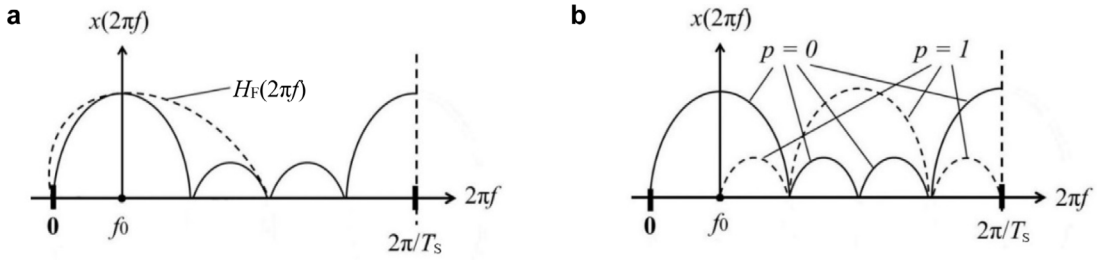

Fig. 4. Spectral characteristics of a signal of the decimation module in a simplified version, at $m = 2$: at the input (a) and at the output (b).

- component in the form of noise in the analyzed frequency spectrum,
- deviations of power frequency values from nominal values in the range of 45–55 Hz.

The quality of digital signal processing can be estimated using a discrete correlation coefficient that characterizes the distortion of the sinusoidality of the analyzed signal and violation of the coherence requirements (Cook and Bernfeld, 1971 [35]; Shirman et al. 2007 [36]).

Note that the probabilistic approach defines the degree of coherence of two centered random variables X and Y (with zero mean) as the value of their correlation coefficient ρ:

$$\rho = \frac{m\{XY^*\}}{\sqrt{\left[m\left\{|X|^2\right\} m\left\{|Y|^2\right\}\right]}} = \frac{R_{XY}}{\sqrt{[R_{XX}R_{YY}]}} \tag{17}$$

where $m\{\ \}$ stands for mathematical mean. For example,

$$R_{XY} = m\left\{XY^*\right\} = \iint_{-\infty}^{+\infty} xy^* p_{xy}(x,\ y)dxdy \tag{18}$$

where p_{xy} is the joint probability density for random variables X and Y, * is the notation for complex conjugate numbers.

It is known that the correlation coefficient satisfies the inequality $0 \le |\rho| \le 1$. Variables X and Y before applying Eq. (18) must be centered by subtracting from each value their respective non-zero mathematical means $m\{X\}$ and $m\{Y\}$. In Eq. (17), R_{XY} is the covariance of variables X and Y.

Practical calculations for sets of values $X(s)$ and $Y(s)$, where s is a variable that characterizes the index of a random value in the set, use the relations

$$|\rho| = \frac{|R_{XY}|}{\sqrt{[R_{XX}R_{YY}]}} \tag{19}$$

where

$$R_{XY} = \frac{1}{N}\sum_{s=1}^{N} X(s)Y^*(s) \tag{20}$$

If $X(s)$ and $Y(s)$ are taken from a set predefined by p_{xy}, then the estimated value R_{XY} (Eq. (20)) tends to R_{XY} (Eq. (18)) in a probabilistic sense at $N \to \infty$.

The degree of coherence is a measure of how closely X and Y are related by a linear transformation. This follows from the analysis of minimum relative mean square error between X and the linear transformation $a \cdot Y$ of Y

$$\min_a m\frac{\left\{|X - a \cdot Y|^2\right\}}{m\left\{|X|^2\right\}} = 1 - |\rho|^2 \tag{21}$$

where the value of a to be minimized is determined by the relation

$$a = \frac{m\{XY^*\}}{m\left\{|Y|^2\right\}} \tag{22}$$

If X and Y are directly related by a linear transformation, then the degree of their coherence is close to its maximum value of 1. A pair of random variables X and Y are assumed to be coherent when $|\rho| = 1$ and incoherent when $|\rho| = 0$.

The degree of coherence of digital processing of signals during their decimation is determined using Eq. (19) for the cross-correlation coefficient. In this case, changes in the cross-correlation coefficient will characterize the signal distortions and the corresponding errors of the IDDS measuring elements. Let us compare the distorted signals with the ideal ones. The ideal signals will be the decimation module input and output signals at $f = 50$ Hz.

5. Voltage signal distortion by harmonics

The base signals for calculating the correlation coefficients will be the sinusoidal signals corresponding to the initial dependence $x(n) = U\cdot \cos(2\pi f_0 n T_S + \varphi)$ and the dependence after decimation $y(k) = U\cdot \cos(8\pi f_0 n T_S + \varphi)$, with time sequences of discrete signal samples. The parameters assumed in the expressions for the base signals are voltage $U =$ 100 V; frequency $f_0 = 50$ Hz; sampling interval $T_S = 1/(f_0\cdot N)$ s; number of samples per power frequency period $N = 80$; initial phase $\varphi = 0$ rad. Oscillograms of signals $x(n)$ and $y(k)$ correspond to Fig. 3.

We will add the 21st harmonic to the initial and thinned signals at a frequency of $f = 42\pi f_0$ with an amplitude of 15 V and evaluate its distorting effect for the two analyzed signals (Fig. 5). Let us assume that the initial phase of the distorting harmonic equals zero.

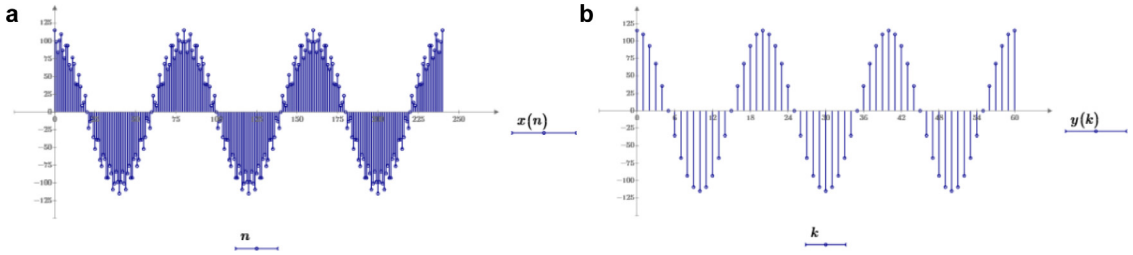

Fig. 5. Oscillograms of a sinusoidal signal distorted by the 21st harmonic before decimation (a) and after decimation (b).

We will simulate the filtering process by the IDDS measuring element, through the DFT for the power frequency harmonic, and determine the amplitudes of the initial $x(n)$ and thinned $y(k)$ signals (Fig. 5).

$$\boldsymbol{S}x = \frac{2}{N}\sum_{n=0}^{N-1}(100\cdot\cos(2\pi f_0 n T_S) + 15\cdot\cos(42\pi f_0 n T_S))\cdot e^{-\frac{j2\pi n}{N}} \tag{23}$$

$$\boldsymbol{S}y = \frac{8}{N}\sum_{k=0}^{(N/4)-1}(100\cdot\cos(2\pi f_0 k 4 T_S) + 15\cdot\cos(42\pi f_0 k 4 T_S))\cdot e^{-\frac{j8\pi k}{N}} \tag{24}$$

The results of calculations using Eqs. (23), (24) show that the amplitudes of the measured fundamental harmonic for the signals $x(n)$ and $y(k)$ (Fig. 5) are different $|\boldsymbol{S}x| = 100$ V, and $|\boldsymbol{S}y| = 115$ V. Thus, the DFT of the decimated signal did not filter out the 21st harmonic, which led to a distortion of the measurement results. The effect generally depends on the relationship between the phases of the fundamental and distorting harmonics and can lead to both an increase and a decrease in the amplitude of the power frequency signal.

Digital processing of analog signals at digital substations using the IEC 61850 SV data exchange protocol often involves merging units (MUs). MUs are used as sources of instantaneous current and voltage values for all technical devices connected to the process bus, which perform the functions of protection, automatic control, remote control, process control systems, power quality control, recording of emergency events oscillograms, and others. Analog-to-digital conversion in MU aims to perform adequate digital processing and playback up to the 50th harmonic. Therefore, not only the 21st but also other harmonics (for example, the 42st harmonic—Fig. 6) will be passed by the MU input circuits and perceived by the measuring element of the IDDSs as a fundamental frequency harmonic for a thinned signal $y(k)$. Note that discrete signals $y(k)$ presented in Figs. 5 and 6 are identical at various distorting disturbances, and oscillograms themselves do not reflect the effect of this impact.

Digital filtering according to Eq. (1) is necessary to ensure the coherence of the digital processing of signal $y(k)$ after decimation. The filtering, however, must be performed for the signal $x(n)$ corresponding to a high sampling rate.

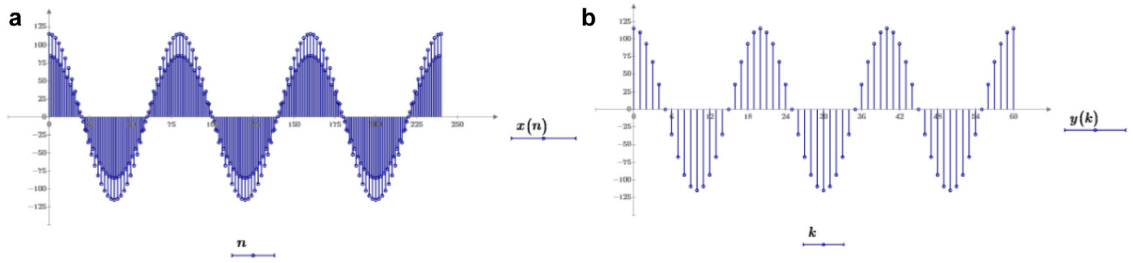

Fig. 6. Oscillograms of a sinusoidal signal distorted by the 42nd harmonic before decimation (a) and after decimation (b).

A comparative analysis of Eqs. (1) and (23) suggests that they are equivalent in terms of computational complexity (number of processing operations), i.e., it is reasonable to estimate the parameters of current and voltage for the signal $x(n)$ with a high sampling rate.

Thus, the decimation procedure and subsequent DFT filtering of the decimated signal for digital substations using the IEC 61850 SV communication protocol leads to the incoherence of digital signal processing and excessive computational load.

The impact of the decimation procedure is assessed only for the power frequency harmonic $f_0 = 50$ Hz with classical DFT. In this case, the effect of the negative influence of distorting signals is scaled to the 2nd, 3rd, and subsequent harmonics.

The influence of interharmonics on the signal during its decimation was investigated by introducing a distorting voltage signal with an amplitude of 15 % of the fundamental harmonic amplitude and a frequency of $f = 39\pi f_0$. Examples of the original and decimated signals are shown in Fig. 7.

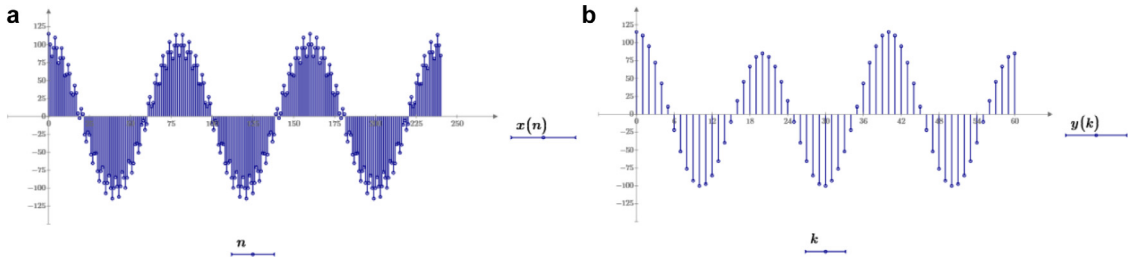

Fig. 7. Oscillograms of a sinusoidal signal distorted by interharmonics at the frequency of $f = 39\pi f_0$ before decimation (a), after decimation (b).

An analysis of the DFT filtering of voltage signals has indicated that the interharmonic has the same distorting effect on both signals $x(n)$ and $y(k)$ and violates their coherence. Comparison of the oscillograms for the signals $x(n)$ and $y(k)$ shown in Fig. 7 illustrates a significant effect typical of power systems with a large share of RPS, which manifests itself in the analysis of causes of emergencies.

Whereas the distortion of sinusoidality of the signal $x(n)$ by harmonic or interharmonic can be observed in oscillogram (Fig. 7), the distortion of the signal $y(k)$ is practically not detected visually. This circumstance can lead to personnel's misinterpretation of the reasons for the activation of the IDDSs, which perform the functions of protection and automatic control, and subsequent incorrect control decisions.

An analysis of the DFT filtering of voltage signals has indicated that the interharmonic has the same distorting effect on both signals $x(n)$ and $y(k)$ and violates their coherence. Comparison of the oscillograms for the signals $x(n)$ and $y(k)$ shown in Fig. 7 illustrates a significant effect typical of power systems with a large share of RPS, which manifests itself in the analysis of causes of emergencies. Whereas the distortion of sinusoidality of the signal $x(n)$ by harmonic or interharmonic can be observed in oscillogram (Fig. 7), the distortion of the signal $y(k)$ is practically not detected visually. This circumstance can lead to personnel's misinterpretation of the reasons for the activation of the IDDSs, which perform the functions of protection and automatic control, and subsequent incorrect control decisions.

Consequently, the insufficient information and analyticity of the oscillograms is an additional disadvantage of the decimation procedure.

Numerically, losses of the coherence of voltage signals are analyzed by comparing the distorted signals for harmonic voltage fluctuations at the power frequency $f_0 = 50$ Hz.

The order of calculations will be illustrated by processing the distorted signal $x(n)$ at the decimation module input. In this case, the expression for calculating the cross-correlation coefficient takes the form

$$|\rho_x| = \frac{|R_{xx_d}|}{\sqrt{\left[R_{xx}\, R_{x_d x_d}\right]}}, \tag{25}$$

where R_{xx_d} is the unnormalized cross-correlation coefficient, R_{xx} and $R_{x_d x_d}$ are autocorrelation coefficients correspond to the energies of voltage signals $x(n)$ and $x_d(n)$.

$$R_{xx_d} = \frac{1}{N}\sum_{s=1}^{N} x(n)x_d(n) = \frac{1}{N}\sum_{s=1}^{N} x(n)\cdot U\cdot\cos(2\pi f_0 n T_s + \varphi) \tag{26}$$

where $x_d(n)$ is the discrete samples of a sinusoidal waveform ($f_0 = 50$ Hz), $\varphi = 0$ rad.

A comparative analysis of Eqs. (23) and (26) shows that the differences between the estimate of the complex amplitude $\boldsymbol{S}x$ and unnormalized cross-correlation coefficient R_{xx_d} lie only in the use of complex arithmetic in Eq. (23). Therefore, the similarity of analyzed expressions confirms the applicability of the cross-correlation coefficient in assessing the coherence of digital signal processing and as a tool for analyzing the magnitude of errors of the IDDS measuring elements. Note that the autocorrelation coefficients R_{xx} and $R_{x_d x_d}$ correspond to the energies of voltage signals $x(n)$ and $x_d(n)$ that include N discrete samples. Similar considerations and calculated relationships can be applied to the signals $y(n)$ and $y_d(n)$. Table 1 shows the calculation results for the normalized cross-correlation coefficient for the decimation options considered above.

Table 1. Calculated values of the normalized cross-correlation coefficient.

No.	Option of voltage signal distortion by harmonics	Normalized cross-correlation coefficient	
		$\|\rho_x\|$	$\|\rho_y\|$
1	The voltage signal distorted by the 21st harmonic corresponding to Fig. 5	0.989	1
2	The voltage signal distorted by the 21st harmonic with the initial phase $\varphi = \pi/4$	0.989	0.995
3	The voltage signal distorted by the 42sn harmonic corresponding to Fig. 6.	0.989	1
4	The voltage signal distorted by interharmonic corresponding to Fig. 7	0.989	0.989

Analysis of the options of voltage signal distortion by harmonic components and interharmonics (Table 1) in the case of decimation has indicated that:

- the calculated normalized cross-correlation coefficient characterizes the probabilistic properties of random processes, while deterministic signals are subjected to analysis, which is why the difference in the obtained numerical values is not large. The relation between the signal energy of the fundamental frequency and the distorting harmonic (signal-to-noise ratio) is high,

- the normalized cross-correlation coefficient can be chosen as a numerical characteristic that allows evaluating the distortion of power frequency signals and characterizing loss of the digital signal processing coherence requirements,

- results of calculations for options 1 and 3 (Table 1) confirm that the coherence requirements are violated during digital processing of a decimated signal. The normalized coefficient of cross-correlation between the distorted power frequency voltage signal and undistorted one, subject to decimation, is 1 (i.e., the signals are similar), and DFT filtering does not eliminate the distorting effect of the 21st and 42nd harmonics,

- comparison of options 1 and 2 (Table 1) confirms that the nature of coherence losses (distortions) depends not only on the energy characteristics of the distortion (the amplitude of the 21st harmonic) but also on phase relationships (initial phase),

- voltage signal distortions by interharmonics for the signals at the decimation module input and output are equivalent.

Analysis of Figs. 4–7 shows that the digital signal processing coherence is violated if the spectrum of the decimated signal contains frequencies greater than half of the reduced sampling rate (i.e., the new Kotelnikov–Nyquist–Shannon-frequency). Their appearance will lead to false frequency components in the spectrum of the

output (decimated) signal of the decimation module. The distorting effect, as in the case of the analog signal sampling, can be eliminated by low-pass prefiltering with a cut-off frequency equal to the Kotelnikov frequency.

In the general case, it is logical to implement low-pass filtering by a non-recursive filter. Firstly, such filtering allows calculating only the required kth thinned samples of the output signal $y(k)$ and ignoring the rest. The recursive filter will not provide such saving on calculations. Secondly, to preserve the phase relationships of the harmonic components of the input signal, it is necessary to use a non-recursive filter with a linear phase response.

6. Distortion of the voltage signal by noise components

Let us consider the voltage signals $xx(n)$ and $yy(k)$, which are a mixture of signals $x(n)$, $y(k)$ and noise in the analyzed bandwidth

$$xx(n) = x(n) + g(n), \quad yy(k) = y(k) + g(k) \tag{27}$$

where $g(n)$ and $g(k)$ are random instantaneous values of noise component.

Fig. 8 shows examples of the original and decimated signal distorted by noise. The results of modeling and calculations according to Eqs. (23) and (24) indicate that the DFT filtering of the original and decimated signals ensures the exclusion of noise components from the power frequency harmonic. Deviations of estimates of signal amplitudes $xx(n)$ and $yy(k)$ depend on the noise intensity and, being equal to a few percentage points, are within the permissible measurement error (Kulikov et al. 2016 [37]). Given that the noise components are random in nature and have both positive and negative values, they can be mutually compensated during summation.

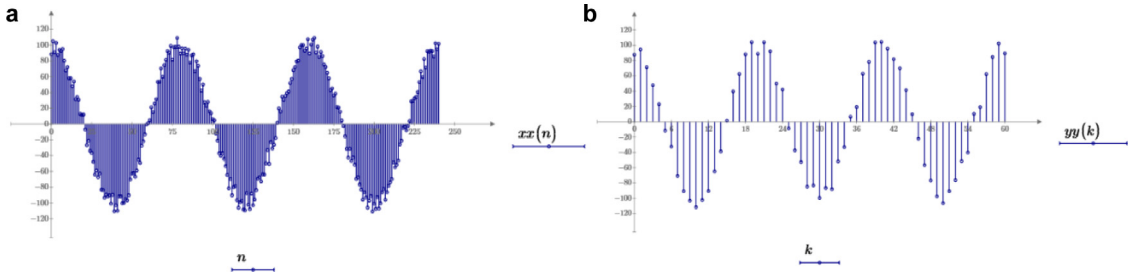

Fig. 8. Oscillograms of a sinusoidal signal distorted by noise before decimation (a) and after decimation (b).

Even with aliased spectra, quasi-coherence of digital signal processing is ensured under the influence of broadband noise. The calculation of the normalized cross-correlation coefficient for signals distorted by noise has shown that $|\rho_{xx}| \approx |\rho_{yy}|$ and are close to unity.

The coherence of digital signal processing, and the accuracy of DFT filtering, are somewhat worse ensured for the signal $yy(k)$ (Fig. 8). This is due to the smaller number of samples used in DFT filtering, and, accordingly, the smaller number of averaged random noise samples.

7. Distortion of the voltage signal with changes in fundamental frequency

Let us investigate the compliance with digital processing coherence requirements for voltage signals $x(n)$ and $y(n)$ (Fig. 3) and their distorted variants (Figs. 5–7) in the case of changes in fundamental frequency. In Borkowski 2007 [14], these distortions are associated with the non-coherent signal sampling caused by the "leakage" effect.

The DFT "leakage" effect is a source of significant errors in frequency analysis in power systems (Rabiner and Gold, 1975 [11]). The "leakage" effect occurs because the DFT spectrum is a convolution of the Fourier transform with a rectangular window function. In the cases where the frequency of the signal component does not match the frequencies of DFT (multiples of the fundamental frequency), the energy of this component is distributed among many other spectral components.

The analysis of current and voltage signals of power frequency normally relies only on the DFT of the first harmonic (Ribeiro et al. 2014 [13]), and the "leakage" effect is associated with incoherent signal sampling. The non-coherent sampling of a current or voltage signal is caused by the fact that the sampling rate in the IDDS, which is usually a constant value, is not synchronized with the changing frequency in the power system. Constant sampling rates are typical of most of the IDDSs that perform the functions of protection, automatic control, measurement,

remote control, electricity metering, process control systems, power quality control, and others (Suslov et al. 2014 [38]).

The lack of synchronization between the sampling rate of the IDDSs and the power frequency signal in the power system leads to a phase error, which is an increasing change in the phase angle in an analysis window with a length equal to the period of a power frequency signal. This effect, along with the DFT "leakage", is a source of significant errors in estimating the operating parameters of the power system at a frequency $f_0 = 50$ Hz (Borkowski, 2007 [14]). Noncoherent sampling rate also causes errors in spectral estimation, detection of harmonic components, measurement of the total harmonic distortion, digital measurements of active/reactive power flows, and others (Xi and Chicharo, 1996 [39]; Arrilaga and Neville, 2003 [40]).

The study the losses of the digital processing coherence are carried out by introducing a discrete signal of the fluctuation frequency f_1 into the model. In the experiments, the values f_1 will be set by extreme numbers of the range 50 ± 5 Hz. Thus, discrete signals, for example, those distorted by the 21st harmonic (Fig. 5) will have the following analytical notation

$$x(n) = 100\cos\left(2\pi(f_0 + f_1)nT_S\right) + 15\cos\left(42\pi(f_0 + f_1)nT_S + \varphi\right) \tag{28}$$

$$y(k) = 100\cos\left(2\pi(f_0 + f_1)k4T_S\right) + 15\cos\left(42\pi(f_0 + f_1)k4T_S + \varphi\right) \tag{29}$$

Fig. 9 shows the examples of original and decimated signals corresponding to Fig. 5 and having a frequency of $f = 45$ Hz, $\varphi = \pi/4$ rad.

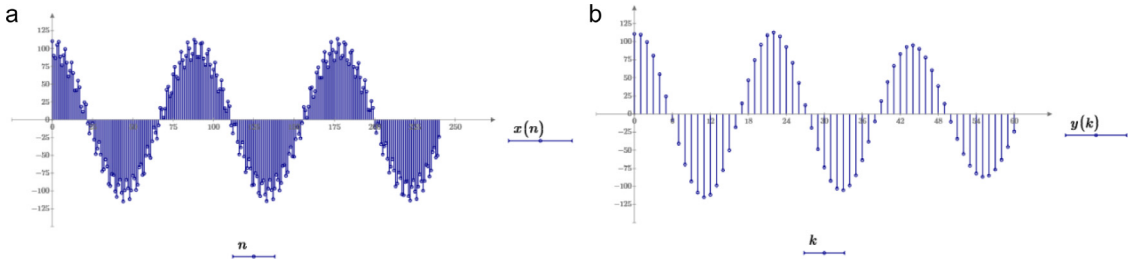

Fig. 9. Oscillograms of a sinusoidal signal, with deviations of the power frequency from $f_0 = 50$ Hz, distorted by the 21st harmonic before decimation (a) and after decimation (b).

Table 2 shows the results of calculations of the normalized cross-correlation coefficient for signals (Figs. 5–7) in the case of the fundamental frequency deviation to the values of $f = 50 \pm 5$ Hz.

Table 2. Calculated values of the normalized cross-correlation coefficient.

No.	Option of the voltage signal distortion by harmonics	Normalized cross-correlation coefficient	
		$\lvert\rho_x\rvert$	$\lvert\rho_y\rvert$
1	Voltage signal distorted by the 21st harmonic, $f = 55$ Hz, $\varphi = 0$ rad	0.939	0.943
2	Voltage signal distorted by the 21st harmonic, $f = 45$ Hz, $\varphi = 0$ rad	0.915	0.958
3	Voltage signal distorted by the 21st harmonic, $f = 55$ Hz, $\varphi = \pi/4$ rad	0.939	0.943
4	Voltage signal distorted by the 21st harmonic, $f = 45$ Hz, $\varphi = \pi/4$ rad	0.915	0.929
5	Voltage signal distorted by the 42nd harmonic, $f = 55$ Hz, $\varphi = 0$ rad	0.938	0.941
6	Voltage signal distorted by the 42nd harmonic, $f = 45$ Hz, $\varphi = 0$ rad	0.915	0.921
7	Voltage signal distorted by the 42nd harmonic, $f = 55$ Hz, $\varphi = \pi/4$ rad	0.939	0.941
8	Voltage signal distorted by the 42nd harmonic, $f = 45$ Hz, $\varphi = \pi/4$ rad	0.914	0.916
9	Voltage signal distorted by interharmonic, $f = 55$ Hz, $\varphi = 0$ rad	0.939	0.919
10	Voltage signal distorted by interharmonic, $f = 45$ Hz, $\varphi = 0$ rad	0.916	0.926
11	Voltage signal distorted by interharmonic, $f = 55$ Hz, $\varphi = \pi/4$ rad	0.939	0.917
12	Voltage signal distorted by interharmonic, $f = 45$ Hz, $\varphi = \pi/4$ rad	0.915	0.927

Analysis of the calculation results given in Table 2 allows the following conclusions:

- digital signal processing in the case of frequency deviations from $f_0 = 50$ Hz causes the effect of "leakage" (incoherence of signal sampling), thereby reducing the cross-correlation coefficient of voltages at the input and

output of the decimation module. "Leakage" effect amplifies the distorting effect for the signals containing high-frequency harmonics,

- deviations of the fundamental frequency up to $f = 55$ Hz and $f = 45$ Hz have different effects on the signal distortion process in the case of decimation. The signals containing the 21st and 42nd harmonics have significantly lower distortion (higher normalized cross-correlation coefficient) than those at a higher frequency ($f = 55$ Hz). When voltage signals are distorted by interharmonic, this relationship is violated,

- analysis of distorting effects should take into account the initial phases of harmonics. Therefore, analyzing power quality indices, one should evaluate not only the energy characteristics of high-frequency harmonic components (for example, the total harmonic distortion) but also their phase relationships,

- at $f_0 = 50$ Hz, the interharmonic component has the same modulating effect on the voltage signals at the input and output of the decimation module. This pattern, however, is not observed when the fundamental frequency deviates up to $f = 55$ Hz and $f = 45$ Hz.

Analytical expressions and simulation results considered in the paper can be used not only to investigate the specific features of digital processing of power frequency signals, but they can also be extended to the study of other technical issues, including bandpass and narrowband filtering, spectral analysis, estimation of signal parameters under noise conditions, and others.

8. Conclusions

The reliable operation of power systems with a large share of renewable power stations the advancement and adoption of digital signal processing methods to prevent failures and unnecessary and false operation of the IDDSs that perform the functions of protection and automatic control.

Digital processing of current and voltage signals of power frequency in IDDSs during decimation must follow coherence requirements. Otherwise, it leads to significant errors in the estimates of the power flow parameters during permanent fluctuations in a wide dynamic range.

A normalized cross-correlation coefficient should be used to determine the extent to which the sinusoidality of current and voltage signals is distorted due to coherence loss during digital signal processing.

The simulation results have indicated that digital processing of signals with frequency deviations from the nominal value is accompanied by the effect of "leakage" (incoherence of signal sampling), thereby reducing the voltage cross-correlation coefficient during decimation. The incoherent sampling increases the distorting effect in the signals with high-frequency harmonic components and interharmonics.

Analysis of the distorting effects on power frequency electrical signals should consider the initial phases of high-frequency harmonic components. Therefore, the assessment of power quality indices should involve not only the energy characteristics of high-frequency harmonic components (for example, the total harmonic distortion) but also their phase relationships.

Declaration of competing interest

The authors declare that they have no known competing financial interests or personal relationships that could have appeared to influence the work reported in this paper.

Data availability

No data was used for the research described in the article.

Acknowledgments

This work is supported by the Russian Science Foundation under grant 21-79-30013 in the Energy Research Institute of the Russian Academy of Sciences.

References

[1] Razavi SE, Rahimi E, Javadi MS, Nezhad AE, Lotfid M, Shafie-khah M, Catalão JPS. Impact of distributed generation on protection and voltage regulation of distribution systems: A review. Renew Sustain Energy Rev 2019;105:157–67. http://dx.doi.org/10.1016/J.RSER.2019.01.050.

[2] Singh B, Sharma J. A review on distributed generation planning. Renew Sustain Energy Rev 2017;76:529–44. http://dx.doi.org/10.1016/J.RSER.2017.03.034.

[3] Mehigana L, Deanea JP, Gallachóira BPÓ, Bertsch V. A review of the role of distributed generation (DG) in future electricity systems. Energy 2018;163:822–36. http://dx.doi.org/10.1016/j.energy.2018.08.022.

[4] Zeng B, Wen J, Shi J, Zhang J, Zhang Y. A multi-level approach to active distribution system planning for efficient renewable energy harvesting in a deregulated environment. Energy 2016;96:614–24. http://dx.doi.org/10.1016/J.ENERGY.2015.12.070.

[5] Ilyushin PV, Kulikov AL, Suslov KV, Filippov SP. Consideration of distinguishing design features of gas-turbine and gas-reciprocating units in design of emergency control systems. Machines 2021;9(3):47. http://dx.doi.org/10.3390/machines9030047.

[6] Degtyarev KS. Renewable energy in Kalmykia: experience, problems and prospects of the region. 2017, URL: https://www.c-o-k.ru/articles/vozobnovlyaemaya-energetika-v-kalmykii-opyt-problemy-i-perspektivy-regiona (accessed: 22/02/2022).

[7] Voropai N, Podkovalnikov S, Osintsev K. From interconnections of local electric power systems to global energy interconnection. Global Energy Interconne 2018;1(1):4–10. http://dx.doi.org/10.14171/J.2096-5117.GEI.2018.01.001.

[8] Papkov B, Gerhards J, Mahnitko A. System problems of power supply reliability analysis formalization. In: Proc. of the 2015 IEEE 5th int. conf. on power engineering, energy and electrical drives. 2015, p. 225–8. http://dx.doi.org/10.1109/PowerEng.2015.7266324.

[9] Voropai N, Podkovalnikov S, Chudinova L, Letova K. Development of electric power cooperation in northeast Asia. Global Energy Interconne 2019;2(1):1–6. http://dx.doi.org/10.1016/J.GLOEI.2019.06.001.

[10] Ilyushin PV, Pazderin AV. Approaches to organization of emergency control at isolated operation of energy areas with distributed generation. in: Proc. of int. ural conf. on green energy. 2018, p. 149-155.

[11] Rabiner LR, Gold B. Theory and application of digital signal processing. Prentice-Hall Inc.; 1975.

[12] Oppenheim AV, Schafer RW. Discrete-time signal processing. 3rd ed. Prentice Hall; 2009.

[13] Ribeiro PF, Duque CA, Silveira PM, Cerqueira AS. Power systems signal processing for smart grids. John Wiley & Sons Ltd.; 2014, http://dx.doi.org/10.1002/9781118639283.

[14] Borkowski D. Estimation of power system spectral parameters with coherent resampling Doctor's Thesis, Cracow, Poland: AGH – Univ. Sci. Technol.; 2007.

[15] Khan Shabbir MNSK, Liang X. A DFFT and coherence analysis-based fault diagnosis approach for induction motors fed by variable frequency drives. In: Proc. of the IEEE canadian conference on electrical and computer engineering. 2020, p. 1–5. http://dx.doi.org/10.1109/CCECE47787.2020.9255688.

[16] Graham MT, Lediju Bell MA. Photoacoustic spatial coherence theory and applications to coherence-based image contrast and resolutionyu. IEEE Trans Ultrason, Ferroelectrics, Frequency Control 2020;67(10):2069–84. http://dx.doi.org/10.1109/TUFFC.2020.2999343.

[17] Ilyushin PV. Emergency and post-emergency control in the formation of micro-grids. E3S Web Conf 2017;25:02002. http://dx.doi.org/10.1051/e3sconf/20172502002.

[18] E. Gurevich Yu, Libova LE. Application of mathematical models of electrical load in calculation of the power systems stability and reliability of power supply to industrial enterprises. Moscow: ELEKS-KM; 2008.

[19] E. Gurevich Yu, Libova LE, Okin AA. Calculations of stability and emergency automation in power systems. Moscow: Energoatomizdat; 1990.

[20] Eroshenko SA, Ilyushin PV. Features of implementing multi-parameter islanding protection in power districts with dis-tributed generation units. In: Proc. of 2018 IEEE 59th int. scientific conf. on power and electrical engineering of riga technical university. 2018, p. 1–6. http://dx.doi.org/10.1109/RTUCON.2018.8659857.

[21] AYu Izmailov, YaP Lobachevsky, Shepovalova OV. Complex energy supply systems for individual sites. Energy Procedia 2019;157:1445–55. http://dx.doi.org/10.1016/j.egypro.2018.11.309.

[22] Shepovalova OV. Mandatory characteristics and parameters of photoelectric systems, arrays and modules and methods of their determining. Energy Procedia 2019;157(2019):1434–44. http://dx.doi.org/10.1016/j.egypro.2018.11.308.

[23] AYu Izmailov, YaP Lobachevsky, Shepovalova OV. Comparison and selection of off-grid pv systems. In: AIP Conf. Proc. 1968. 2018, 030001. http://dx.doi.org/10.1063/1.5039188.

[24] Strebkov DS, Shepovalova OV, NIu Bobovnikov. Investigation of high-voltage silicon solar modules. AIP Conf Proc 2019;2123(2019):020103. http://dx.doi.org/10.1063/1.5117030.

[25] Ren J, Kezunovic M. An adaptive phasor estimator for power system waveforms containing transients. IEEE Trans Power Deliv 2012;27(2):735–45. http://dx.doi.org/10.1109/TPWRD.2012.2183896.

[26] Serna JADLO, Martin KE. Improving phasor measurements under power system oscillations. IEEE Trans Power Syst 2003;18(1):160–6. http://dx.doi.org/10.1109/TPWRS.2002.807033.

[27] Serna JADLO. Dynamic phasor estimates for power system oscillations. IEEE Trans Instrum Meas 2007;56(5):1648–57. http://dx.doi.org/10.1109/TIM.2007.904546.

[28] Kulikov AL, Lukicheva IA. Application of a multimodel approach for estimating the frequency of an electric network. in: Proc. of XLVIII international scientific and practical conference with elements of a scientific school. 2018, p. 259-265.

[29] Antonov VI. Adaptive structural analysis of electrical signals: theory and its applications in intelligent electric power engineering. Cheboksary: Publishing house of the Chuvash State University; 2018.

[30] Buchholz BM, Styczynski Z. Smart grids – fundamentals and technologies in electricity networks. New York: Springer Heidelberg; 2014.
[31] Shushpanov I, Suslov K, Ilyushin P, Sidorov D. Towards the flexible distribution networks design using the reliability performance metric. Energies 2021;14(19):6193. http://dx.doi.org/10.3390/en14169854.
[32] Goldenberg LM, Matyushkin BD, Polyak MN. Digital signal processing: handbook. Moscow: Radio and Communications; 1985.
[33] Hu JS, Lee MT. Multi-channel post-filtering based on spatial coherence measure. Signal Process 2014;105:338–49. http://dx.doi.org/10.1016/j.sigpro.2014.04.020.
[34] Li F, Zou L, Songa J, Liang S, Chen Y. Investigation of the spatial coherence function of wind loads on lattice frame structures. J Wind Eng Ind Aerodyn 2021;215:104675. http://dx.doi.org/10.1016/J.JWEIA.2021.104675.
[35] E. Cook Ch, Bernfeld M. Radar signals:An introduction to theory and application. Academic Press; 1971, http://dx.doi.org/10.1016/B978-0-12-186750-8.X5001-7, 1967.
[36] D. Shirman Ya, Bagdasaryan ST, Malyarenko AS. Radio-Electronic Systems: Fundamentals of Construction and Theory: Handbook. 2nd ed.. Moscow: Radio Engineering; 2007, transl. and additional..
[37] Kulikov AL, Anan'ev VV, Vukolov VY, Platonov PS, Lachugin VF. Modelling of wave processes on power transmission ines to improve the accuracy of fault location. Power Technol Eng 2016;49(5):378–85. http://dx.doi.org/10.1007/s10749-016-0632-8.
[38] Suslov KV, Solonina NN, Smirnov AS. Distributed power quality monitoring. In: Proc. IEEE 16th International conference on harmonics and quality of power. 2014, p. 517–20. http://dx.doi.org/10.1109/ICHQP.2014.6842882.
[39] Xi J, Chicharo JF. A new algorithm for improving the accuracy of periodic signal analysis. IEEE Trans Instrum Meas 1996;45(4):109–15. http://dx.doi.org/10.1109/19.517004.
[40] Arrilaga J, Neville WR. Power system harmonics. chichester. U.K: Wiley; 2003.